Optical control of the spin of a magnetic atom in a semiconductor quantum dot

Lucien Besombes, Hervé Boukari, Claire Le Gall, Adalberto Brunetti, Chong Long Cao, Ségolène Jamet, Bobin Varghese

Optical control of the spin of a magnetic atom in a semiconductor quantum dot

L. Besombes,[1,2,*] H. Boukari,[1,2] C. Le Gall,[1,2] A. Brunetti,[1,2] C.L. Cao,[1,2] S. Jamet,[1,2] and B. Varghese[1,2]

[1] *CNRS, Institut Néel, F-38042 Grenoble, France.*
[2] *Univ. Grenoble Alpes, Institut Néel, F-38042 Grenoble, France*

(Dated: November 26, 2014)

The control of single spins in solids is a key but challenging step for any spin-based solid-state quantum-computing device. Thanks to their expected long coherence time, localized spins on magnetic atoms in a semiconductor host could be an interesting media to store quantum information in the solid state. Optical probing and control of the spin of individual or pairs of Mn atoms (S=5/2) have been obtained in II-VI and III-V semiconductor quantum dots during the last years. In this paper, we review recently developed optical control experiments of the spin of an individual Mn atoms in II-VI semiconductor self-assembled or strain free quantum dots. We first show that the fine structure of the Mn atom and especially a strained induced magnetic anisotropy is the main parameter controlling the spin memory of the magnetic atom at zero magnetic field. We then demonstrate that the energy of any spin state of a Mn atom or pairs of Mn atom can be independently tuned by using the optical Stark effect induced by a resonant laser field. The strong coupling with the resonant laser field modifies the Mn fine structure and consequently its dynamics. We then describe the spin dynamics of a Mn atom under this strong resonant optical excitation. In addition to standard optical pumping expected for a resonant excitation, we show that the Mn spin population can be trapped in the state which is resonantly excited. This effect is modeled considering the coherent spin dynamics of the coupled electronic and nuclear spin of the Mn atom optically dressed by a resonant laser field. Finally, we discuss the spin dynamics of a Mn atom in strain free quantum dots and show that these structures should permit a fast optical coherent control of an individual Mn spin.

I. INTRODUCTION

The ability to control individual spins in semiconductor nanostructures is an important issue for spintronics and quantum information processing[1]. Thanks to their expected long coherence time, localized spins on magnetic atoms in a semiconductor host could be an interesting media to store quantum information in the solid state. However, probing the spin of an individual magnetic atom in a diluted magnetic semiconductor (DMS)[3] remained a challenge for many years before the development of DMS based quantum dots (QDs)[2]. Optically controlled semiconductor QDs are in many ways similar to atomic systems. In the recent years several quantum optics effects first demonstrated in atoms have been observed on individual QDs. For instance, resonant optical pumping[4] has been successfully used to prepare the spin of an individual electron[5] or hole[6] localized in a QD. The possibility to use a strong resonant continuous wave laser field to create hybrid matter-field states[7] and manipulate QDs states in their solid environment has also been demonstrated in different QD systems[8]. The Autler-Townes effect in the fine structure of a neutral or charged QD[9,10], the Mollow absorption spectrum of an individual QD[11] and the emission of an optically dressed exciton and biexciton complex[12] have been reported. Exploiting these optical properties of QDs, it has been demonstrated during the last years the possibility to optically probe and control the spin of individual or pairs of Manganese (Mn) atoms both in II-VI[13,14] and III-V[15–17] DMS. Recently, other magnetic elements, like Co, have also been successfully incorporated in II-VI semiconductor QDs[18].

When a single Mn atom is included in a II-VI semiconductor QD, the spin of the optically created electron-hole pair (exciton) interacts with the five d electrons of the Mn (total spin S=5/2). This leads to a splitting of the once simple photoluminescence (PL) spectrum of an individual QD (Fig. 1(a)) into six (2S+1) components (Fig. 1(b)). This splitting results from the spin structure of the confined heavy holes which are quantized along the QDs growth axis with their spin component taking only the value $J_z=\pm 3/2$. In first approximation, the hole-Mn exchange interaction reduces to an Ising term $J_z S_z$ and shifts the emission energy of the QD, depending on the relative orientation of the spin of the Mn (S_z) and hole (J_z)[19–22]. As the spin state of the Mn atom fluctuates during the optical measurements, the six lines are observed simultaneously in time-averaged PL spectra. The intensities of the lines reflect the probability for the Mn to be in one of its six spin components when the exciton recombines[23,24]. II-VI semiconductor QDs with 2 Mn atoms give more complex spectra with up to 36 lines (Fig. 1(c)) but the two localized spins can still be addressed using similar optical techniques[14]. If a third Mn atom interacts with the exciton, 6×36 emission lines are expected. As the typical PL linewidth in CdTe/ZnTe QDs is larger than the line spacing, the detail of the emission structure of such QD cannot be resolved. A broad emission line is obtained and the 3 Mn case can be hardly distinguished from a QD containing a larger number of magnetic atoms[25].

In this review we present different optical techniques allowing probing and controlling the spin of an individ-

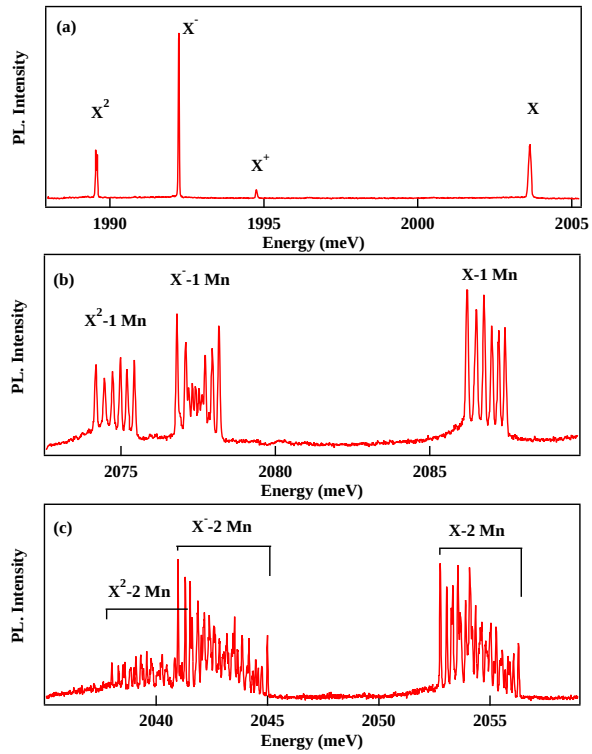

FIG. 1: Low temperature (T=5K) PL spectra of three different CdTe/ZnTe QDs containing 0 (a), 1 (b) and 2 (c) Mn atoms and a variable number of carriers (one electron-hole pair (X), two electron-hole pairs (X^2), two electrons one hole (X^-) and one electron two holes (X^+)). All the spectra are obtained under resonant excitation on an excited state of the dots.

ual magnetic atom in self-assembled and strain free QDs. We first show that the fine structure of the Mn atom and especially a strained induced magnetic anisotropy is the main parameter controlling the spin memory of the magnetic atom at zero magnetic field. We then demonstrate that the energy of any spin state of a Mn atom or pairs of Mn atoms can be independently tuned by using the optical Stark effect induced by a resonant laser field. The strong coupling with the resonant laser field modifies the Mn fine structure and consequently its dynamics. We then describe the spin dynamics of a Mn atom under this resonant optical excitation. In addition to standard optical pumping expected for a resonant excitation, we show that the Mn spin population can be trapped in the state which is resonantly excited. This effect is modeled considering the coherent spin dynamics of the coupled electronic and nuclear spin of the Mn atom optically dressed by a resonant laser field. Finally, we discuss the spin dynamics of a Mn atom in strain free quantum dots and show that these structures should permit an optical coherent control of an individual Mn spin.

II. MN SPIN STRUCTURE AND DYNAMICS IN A SELF-ASSEMBLED QUANTUM DOT

The localisation of a magnetic atom in a QD enhances its exchange interaction with the spin of the carriers of the host semiconductor allowing probing the spin state of an individual atom. Cd(Mn)Te DMS QDs are grown by molecular beam epitaxy on a ZnTe (self-assembled QDs[26]) or on a CdTe substrate (strain free QDs[27]). A low density of Mn atoms is introduced during the growth of the thin CdTe QD layer. Non-magnetic and magnetic QDs containing a small number of Mn atoms (1,2,3 ...) are then formed. Optical addressing of individual QDs is achieved using micro-spectroscopy techniques. A high refractive index hemispherical solid immersion lens is mounted on the surface of the sample to enhance the spatial resolution and the collection efficiency of single dot emission in a low-temperature (T=5K) scanning optical microscope. This technique also reduces the reflected and scattered light at the sample surface allowing the measurement of spin-flip scattered photons from a Mn-doped QD[28]. Individual QDs are excited with tunable continuous wave lasers tuned to an excited state of the dots or on resonance with the QD' s-state[29].

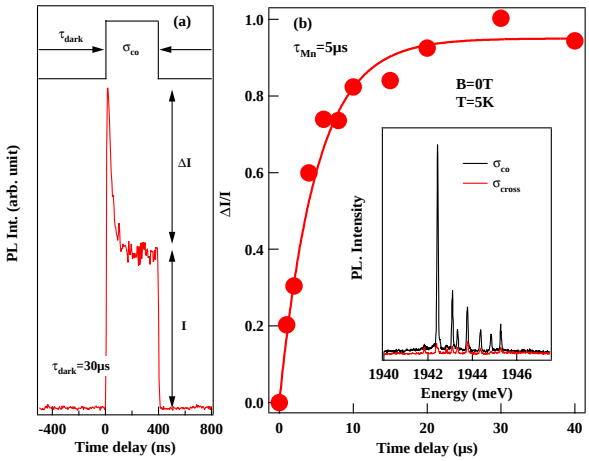

FIG. 2: (a) Time evolution of the PL intensity recorded at B=0T and T=5K on the high energy line of a Mn-doped QD under the quasi-resonant (QD excited state) excitation sequence displayed on the top. An intensity transient induced by the optical pumping of the Mn spin appears at the beginning of the circularly polarized excitation pulse. (b) Evolution of the amplitude of the optical pumping transient $\Delta I/I$ as a function of the dark time between the excitation pulses. A relaxation time $\tau_{Mn} = 5\mu s$ is measured at B=0T. The inset shows the co and cross circularly polarized PL of the exciton-Mn complex.

In the case of singly Mn-doped QDs, circularly polarized light can be used to efficiently control the occupation of the Mn spin states[30–34]. To optically pump the Mn spin, the QD is excited with a tunable continuous wave laser on resonance with an excited state. The relative

intensity of the PL lines of the exciton-Mn (X-Mn) state depends strongly on the correlation between the polarization of the excitation and detection (inset of Fig. 2(b)). As each line corresponds to a given spin state of the Mn, S_z, this shows that the whole process of optical spin injection and relaxation creates a non-equilibrium distribution of the Mn spin states.

With this method to prepare the Mn spin, we can perform pump-probe experiments to observe how long the Mn polarization can be conserved (Fig. 2). We prepare a non-equilibrium distribution of the Mn spin with a circularly polarized pump pulse. This spin orientation takes place in a time-scale of a few tens of nanoseconds, depending on the laser excitation intensity. The pump laser is then switched off, and switched on again after a dark time τ_{dark}. The amplitude of the pumping transient after τ_{dark} depends on the Mn spin relaxation in the dark. For the QD presented in Fig. 2, the amplitude of the transient is fully restored after 20 μs. From the delay dependence of this amplitude we deduce a Mn relaxation time $\tau_{Mn} = 5\mu s$. This spin relaxation time changes from dot to dot as is not an intrinsic property of the magnetic atom[28,31].

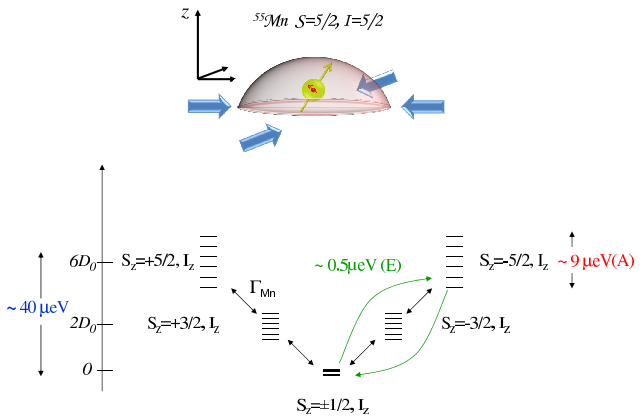

FIG. 3: Scheme of the energy level of a Mn atom in a strained II-VI QD. All the stable Mn isotopes ^{55}Mn carries a nuclear spin I=5/2 which couples through hyperfine interaction (A I.S) to the electronic spin S=5/2. The d orbital of the Mn is also sensitive to the electric field produced by the neighboring atoms (crystal field) in the zinc-blende lattice. A distortion of the lattice and consequently a change in the crystal field will also affect the d orbital. The dynamic of the Mn spin at zero magnetic field is mainly controlled by a magnetic anisotropy D_0 produced by the presence of large bi-axial strain at the Mn location. This crystal field splits the spin states of the Mn according to $D_0 S_z^2$. Anisotropy of the strain in the quantum dot plane ($E(S_x^2\text{-}S_y^2)$) also mix different S_z components (green arrows).

To understand the spin dynamics of a Mn atom and the detail of the optical properties of Mn-doped QDs, we have to notice that all the stable Mn isotopes (^{55}Mn) carries a nuclear spin I=5/2 which couples through hyperfine interaction to the electronic spin S=5/2. The d orbital of the Mn is also sensitive to the electric field produced by the neighboring atoms (crystal field) in the zinc-blende lattice. A distortion of the lattice and consequently a change in the crystal field will also affect the d orbital. The Hamiltonian of the coupled electronic and nuclear spins of a Mn atom in a strained layer grown along [001] axis is known from magnetic resonance measurements[35] and reads:

$$\begin{aligned}\mathcal{H}_{Mn} &= \mathcal{A}\vec{I}.\vec{S} \\ &+\frac{1}{6}a[S_x^4+S_y^4+S_z^4-\frac{1}{5}S(S+1)(3S^2+3S-1)] \\ &+\mathcal{D}_0[S_z^2-\frac{1}{3}S(S+1)]+E[S_x^2-S_y^2] \\ &+g_{Mn}\mu_B\vec{B}.\vec{S} \qquad (1)\end{aligned}$$

where $\mathcal{A}$ is the hyperfine coupling ($\mathcal{A} \approx +0.7\mu eV$)[36,37], which results from the magnetic dipolar interaction between the Mn $5d$ electrons forming the total spin $\vec{S}$ and the spin of the Mn nucleus $\vec{I}$ (I=5/2). The second term of the Hamiltonian comes from the cubic symmetry of the crystal field and mixes different S_z of the Mn spin. We have $a = 0.32\mu eV$ according to reference[35].

The presence of bi-axial strains in the QD plane leads to the magnetic anisotropy term with $\mathcal{D}_0 \approx 12\mu eV$ for a fully strained CdTe layer matched on a ZnTe substrate. Because of partial relaxation of the strain during the growth process, weaker values of $\mathcal{D}_0$ are usually observed in self-assembled QDs[31]. An anisotropy of the strain in the xy plane (QD plane) can mix different S_z components through the anisotropic crystal field. This coupling is described in the Hamiltonian (1) by its characteristic energy E which depends on the local strain distribution at the Mn atom location.

In highly strained QDs at zero magnetic field, the Mn electronic spin is quantized along the growth axis z and the different electronic spin doublets (S_z=±1/2, S_z=±3/2 and S_z=±5/2) are separated by an energy proportional to $\mathcal{D}_0$ (Fig. 3). The S_z=±5/2 and S_z=±3/2 doublets are split into six lines by the hyperfine coupling with the nuclear spin I=5/2. For the doublet S_z=±1/2, the isotropic coupling with the nuclear spin I=5/2 results in two levels with total spin M=2 and M=3.

In the presence of magnetic anisotropy, the precession of the electronic Mn spin in its hyperfine nuclear field is blocked even at B=0 T. The Mn atom has to interact with phonons to relax its electronic spin which is not an efficient process for a pure spin (no orbital momentum)[38–40]. This is responsible for the Mn spin memory observed at zero magnetic field in self-assembled QDs.

III. OPTICAL STARK EFFECT ON AN INDIVIDUAL MN SPIN

The fine and hyperfine structure of a Mn atom embedded in a II-VI semiconductor QD can be tuned using the optical Stark effect induced by a strong laser field[41]. To demonstrate this effect, single QD PL is excited with a continuous wave dye laser tuned to an excited state of the QD[29]. Simultaneously, a tunable continuous wave single-mode dye ring laser, named control laser in the following, is used to resonantly excite the excitonic transitions. The resulting circularly polarized collected PL is dispersed and filtered by a 1 m double monochromator before being detected by a cooled CCD camera.

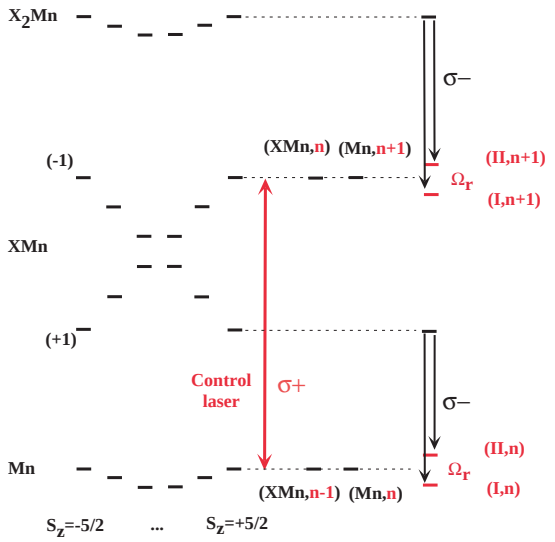

FIG. 4: Energy scheme of a Mn-doped QD and formation of light-matter hybrid states by a laser field. In the absence of carriers, the Mn fine structure is dominated by the strain induced magnetic anisotropy which also splits the biexciton states (X_2Mn). The bright exciton levels (X, with kinetic momentum ± 1) are split by the exchange interaction with the Mn (XMn levels). A pump laser tuned to a QD excited state is used to produce PL of any exciton and biexciton states. The Rabi splitting, $\hbar\Omega_r$, induced on the Mn state by the control laser (circularly polarized $\sigma+$) can be probed in the PL of the exciton while the splitting of XMn is observed in the PL of the biexciton. (I,n), (II,n), (I,n+1) and (II,n+1) are the optically dressed states produced by the mixing of the uncoupled states (XMn,n-1), (Mn,n), (XMn,n) and (Mn,n+1) where n is the number of photons in the control laser.

Only one spin state of the Mn is addressed when a control laser is circularly polarized ($\sigma\pm$) and tuned on resonance with an emission line of the exciton-Mn (XMn) complex. As illustrated in Fig. 4, the influence of the control laser tuned to the high energy line of XMn in $\sigma+$ polarization can be detected in $\sigma-$ polarization on the low energy line of XMn. In the strong coupling regime, the control laser induces a splitting of the resonantly excited level similar to the Autler-Townes splitting observed in atomic physics[42]. The control laser field mixes the states with a Mn spin component S_z=+5/2 in the presence (XMn) or absence (Mn) of the exciton. At the resonance, the unperturbed states $|Mn\rangle \otimes |n\rangle$ and $|XMn\rangle \otimes |n-1\rangle$ can be dressed into pairs of hybrid matter-field states $|I,n\rangle$ and $|II,n\rangle$ where $|n\rangle$ is a n-photons state of the control laser (see Fig. 4). These states can be written as[43]:

$$|I,n\rangle = c|Mn\rangle \otimes |n\rangle - s|XMn\rangle \otimes |n-1\rangle$$
$$|II,n\rangle = s|Mn\rangle \otimes |n\rangle + c|XMn\rangle \otimes |n-1\rangle$$

with corresponding energies $E_\pm = \frac{\hbar}{2}(\omega_c + \omega_0) \pm \frac{\hbar}{2}\Omega'_r$. Here, $c = \sqrt{\frac{1}{2}(1 - \frac{\delta}{\Omega'})}$ and $s = \sqrt{\frac{1}{2}(1 + \frac{\delta}{\Omega'})}$. $\delta = \omega_c - \omega_0$ is the laser detuning with ω_0 the resonance frequency of the unperturbed transition and ω_c the frequency of the control laser. $\hbar\Omega'_r = \hbar\sqrt{\Omega_r^2 + \delta^2}$ defines the energy splitting of the dressed states where $\Omega_r = \mathcal{P}\mathcal{E}/\hbar$ is the Rabi frequency with $\mathcal{P}$ the dipolar moment of the QD transition and $\mathcal{E}$ the amplitude of the electric field of the control laser. A power dependent Autler-Townes type splitting is then expected for all transitions that share such an optically dressed state[7,42].

Experimental data corresponding to a control laser tuned on $|+1,+5/2\rangle$ and the observation of an Autler-Townes splitting in the PL of the state $|-1,+5/2\rangle$ are presented in Fig. 5. Particular care is given to the effect of the detuning of the control laser from the XMn resonance (Fig. 5(c) and 5(d)) and its intensity (Fig. 5(e) and 5(f)). At large laser detuning, the optically active transitions asymptotically approach the original excitonic transitions where the remaining energy offset is the optical Stark shift. At the resonance, an anti-crossing is observed showing that the strong coupling between the laser field and the exciton creates hybrid light-matter states.

As presented in the inset of Fig. 5(d), a good agreement with the simple dressed atom model is obtain with a Rabi energy of $\hbar\Omega_r$=180μeV. On resonance, the emission from the $|-1,+5/2\rangle$ state splits into a doublet when the power of the control laser is increased, as expected from the Autler-Townes model. The splitting is plotted as a function of the square root of the control laser intensity in Fig. 5(f), showing that the splitting linearly depends on the laser field strength. A Rabi splitting larger than 250μeV is obtained at high excitation intensity. It is worth noting that these energy shifts can be easily larger than the magnetic anisotropy of an isolated Mn spin created by the strain in the QD plane ($\approx$40μeV)[31,32,35]. This optical tuning of the fine structure may lead to a control of the coherent dynamics of the isolated Mn spin.

The high energy transition of the XMn complex is twice degenerated. The corresponding optical transitions differ by the polarization of the absorbed or emitted photons. The polarization dependence of the laser induced splitting shown in Fig. 5(b) confirms the Mn spin selectivity of the strong coupling with the laser field: $\sigma+$ photons couple with the state $|+5/2\rangle$ of the Mn to create

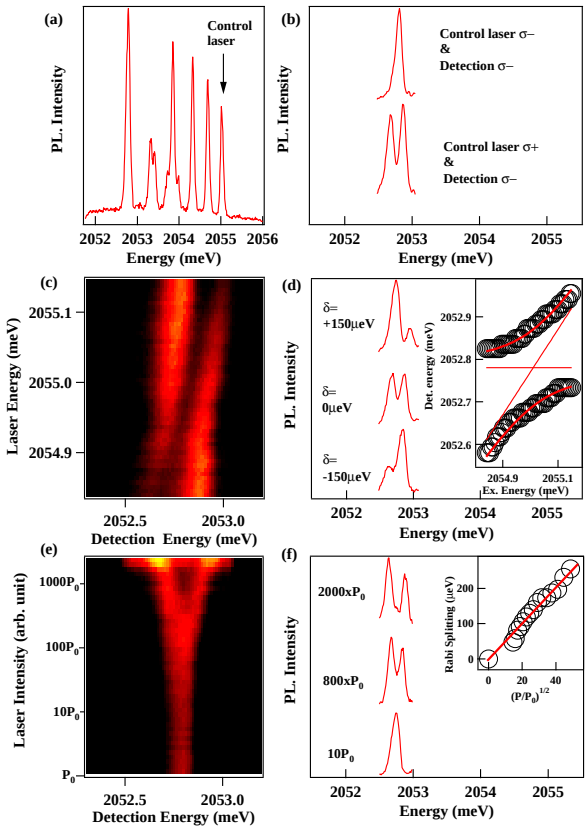

FIG. 5: Autler-Townes splitting of the emission of $|-1,+5/2\rangle$ in a Mn-doped QD resonantly excited on $|+1,+5/2\rangle$. (a) shows the non-resonant PL of the QD. (b) presents the circular polarisation dependence of the Rabi splitting obtained under resonant excitation. The intensity map (c) shows the excitation energy dependence of the Rabi splitting. The corresponding emission line-shape is presented in (d). The inset shows the spectral position of the Autler-Townes doublet as a function of the pump detuning. The fit is obtained with a Rabi energies $\hbar\Omega_r = 180\mu eV$. The straight lines corresponds to the uncoupled exciton and laser energy. The excitation intensity dependence of the Autler-Townes doublet is presented in the intensity map (e). The corresponding emission line-shape are presented in (f). The inset shows the evolution of the Rabi splitting as a function of the square-root of the pump intensity.

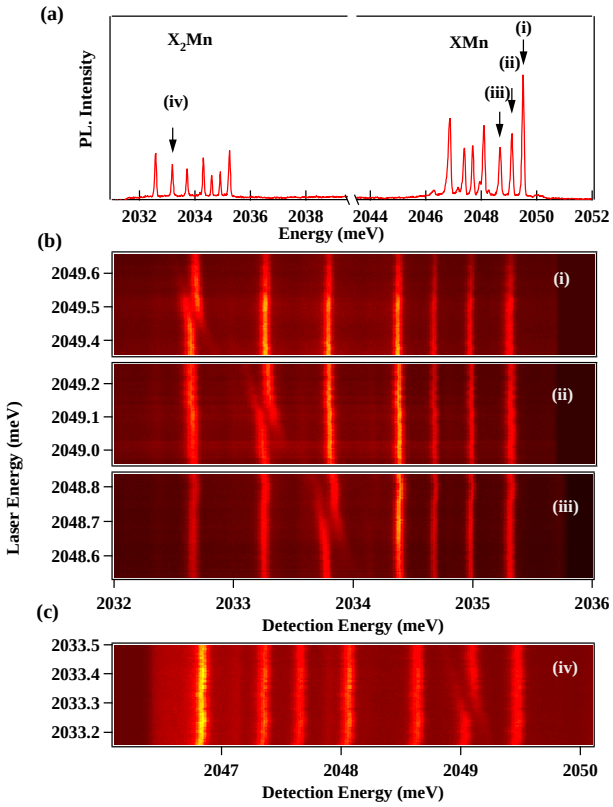

FIG. 6: (a) PL of the exciton and biexciton in a Mn-doped QD. (b) Autler-Townes splitting of the exciton detected on the biexciton PL under resonant excitation of the ground-to-exciton transition for the spin state of the Mn S_z=+5/2 (i), S_z=+3/2 (ii) and S_z=+1/2 (ii) (arrows in the PL spectra). (c) Emission of the exciton for a dressed exciton-to-biexciton transition. The excitation is tuned around the state S_z=+3/2 of the biexciton (iv).

two hybrid light-matter states while no splitting of the $\sigma-$ PL line is observed with $\sigma-$ control photons.

The strong coupling with the control laser is also observed in optical transitions that involve the biexciton exchanged coupled to a single Mn (X_2Mn). This is illustrated in Fig. 6 in the case of successive resonant excitations on the XMn levels with a Mn spin state S_z=+1/2, +3/2 and +5/2. In these cases, the recombinaison of X_2Mn probes the laser induced splitting of XMn for a given spin states of the Mn. It is shown here that any XMn transition, and consequently any Mn spin state, can be optically shifted by a control laser tuned on resonance. As illustrated in Fig. 6(c), by coherently driving the X_2Mn-to-XMn transition, one can also tune the energy of any state of the XMn complex. This set of experiment demonstrates that a complete optical control of the exciton-Mn system is possible.

To summarize, the Mn ground state, exciton and biexciton states in a Mn-doped QD can be coherently manipulated by applying a strong resonant laser field on the optical transitions. The transition in a Mn-doped QD behaves like isolated two-level quantum systems well described by the dressed atom picture. At the resonance with an exciton transition, hybrid matter-field states are created that should significantly influence the Mn spin dynamics.

IV. SPIN DYNAMICS OF AN OPTICALLY DRESSED MN ATOM.

In order to observe the population distribution on the spin states of the Mn under resonant optical excitation on a given X-Mn level, we developed a technique allowing

probing simultaneously the six spin states in the resonant optical excitation regime[44]. The principle of this experiment is presented in Fig. 7. It is based on the creation of a biexciton by a two-photon absorption process under resonant pulsed excitation for the Mn spin readout, combined with a continuous wave (CW) resonant excitation on X-Mn for the Mn spin preparation.

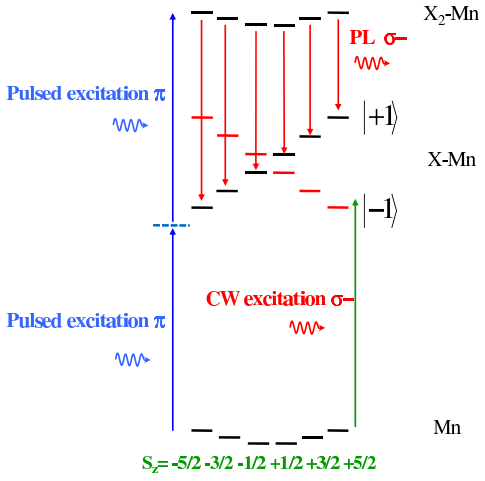

FIG. 7: Scheme of the optical transitions and their polarizations in a quantum dot containing an individual magnetic atom and 0 (Mn), 1 (X-Mn) or 2 (X_2-Mn) excitons. The exciton states are split by the exchange interaction with the Mn spin whereas in the ground (Mn) and biexciton (X_2-Mn) states the energy levels results from the fine and hyperfine structure of the Mn spin. A direct resonant excitation of the biexciton is performed by a pulsed two-photon absorption through an intermediate virtual state whereas X-Mn states a resonantly excited by a tunable CW laser.

A picosecond pulsed laser excitation tuned between the exciton and the biexciton transitions can directly create a biexciton in a QD through a two-photon transition[45]. As the biexciton is a spin singlet state (2 paired electrons and 2 paired holes), in a first approximation it does not interact with the Mn spin[46]. The population distribution on the six Mn spin states is then extracted from the intensity of the PL lines of the biexciton which is controlled by X-Mn in the final state of the biexciton recombination. As the emission of the biexciton is shifted by 10 to 14 meV below the resonant excitation on the X-Mn levels, it can be easily separated from the scattered photons of the CW pumping laser. The resonant two-photon absorption scheme used here also avoids the injection of free carriers in the vicinity of the QD and consequently limits the spin relaxation of the Mn by exchange coupling with these free carriers[23]. Let us note however that the cascade recombination of the biexciton leaves in the QD a maximum of one exciton every 13 ns (repetition rate of the pulsed excitation). These excitons with a characteristic X-Mn spin flip time of about 50ns[28] may slightly perturb the Mn spin preparation. However, as we will see, a signature of the resonant preparation of the Mn is clearly observed in the biexciton signal which appears as a good probe of the Mn spin population.

The experimental evidence of the two-photon resonant formation of X_2-Mn is presented in Fig. 8. As expected from optical selection rules of the two-photon transition[45], PL from X_2-Mn can only be observed with linearly polarized laser pulses tuned in between the exciton and biexciton transitions. Excitation with circularly polarized pulses do not create any significant QD luminescence. This confirms that one can find experimental conditions where the PL from the QD is dominated by the two-photon resonant excitation. The non-resonant creation of free carriers in the QD vicinity is very weak and will not perturb the Mn spin dynamics.

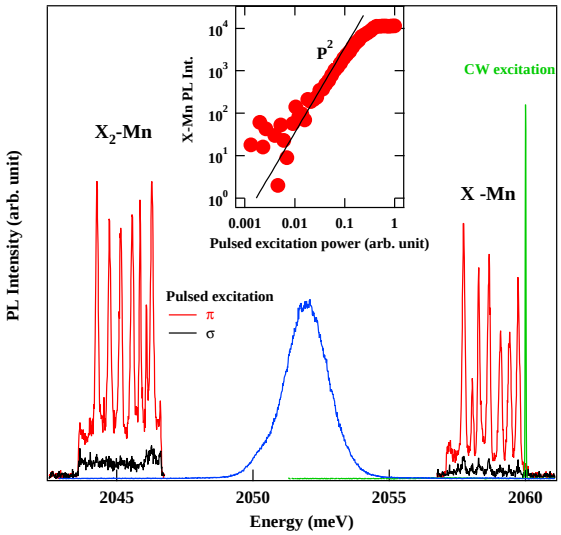

FIG. 8: PL spectra of a Mn-doped QD obtained under a two-photon resonant absorption of a picosecond laser pulse (spectra of the pulsed laser in blue). The resonant creation of the biexciton (X_2-Mn) is only possible for a linearly polarized excitation (red) whereas almost no PL is observed for circularly polarized pulses (black). The influence on the Mn spin population of a CW control laser (spectra of the CW laser in green) in resonance with the exciton (X-Mn) levels can be detected in the intensity distribution of X_2-Mn. Inset: PL intensity of X-Mn versus the intensity of the pulsed linearly polarized excitation. The P^2 dependence is characteristic of a two-photon absorption.

The intensity distribution of the X_2-Mn created by the two-photon absorption scheme presented above allows to probe the preparation of the Mn spin by the CW control laser near the resonance with X-Mn states. Fig. 9 presents resonant optical experiments performed under co and cross circular polarization for the resonant CW excitation and the two-photon detection of X_2-Mn. Without CW resonant excitation on X-Mn, an identical intensity is observed for the six main lines of X_2-Mn PL showing that the two-photon excitation does not have any significant effect on the Mn spin population. A strong

change in the intensity distribution is observed when the CW laser is scanned across each X-Mn level suggesting a complex Mn spin dynamics.

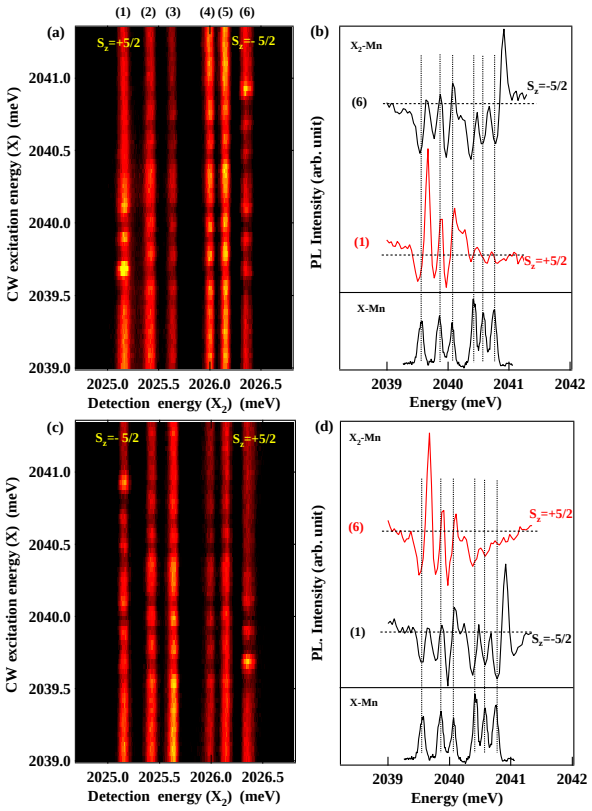

FIG. 9: Map of the PL intensity of X_2-Mn versus the energy of the CW resonant excitation on X-Mn for co (a) and cross (c) circular CW excitation and detection of X_2-Mn. (b) and (d) present the corresponding intensity curves of X_2-Mn for the spin states S_z=+5/2 (1) and S_z=-5/2 (6).

With circularly polarized photons, an excitation on a given X-Mn level only affects one spin state of the Mn. For co-circular excitation on X-Mn and detection on X_2-Mn, the low energy lines of X-Mn and X_2-Mn correspond to the same spin state of the Mn (see the level scheme presented in Fig. 7). As presented in Fig. 9, when a CW excitation laser is scanned around the low energy line of X-Mn, it mainly affects the low energy line of X_2-Mn. Similarly, as the high energy line of X-Mn is excited, the intensity of the high energy line of X_2-Mn is significantly modified. Both configurations show that the resonant CW excitation mainly affects the spin state of the Mn which is resonantly excited.

To analyze the details of the influence of the CW resonant laser on the Mn spin population, we focus on the two outside lines of the PL of X_2-Mn. They correspond to the spin states $S_z = +5/2$ or $S_z = -5/2$. The intensity of these lines is presented in Fig. 9(b) versus the energy of the resonant CW laser. As expected for an optical spin pumping mechanism, one observes a decrease of the S_z=+5/2 spin population when the laser is tuned on resonance with the X-Mn level $|J_z = -1, S_z = +5/2\rangle$. However, a strong increase of the S_z=+5/2 population is observed when the CW control laser is slightly detuned on the high energy side of the X-Mn optical transition. A similar behavior is observed when the high energy line of X-Mn is excited and the high energy line of X_2-Mn is probed (i.e. exciting and detecting the Mn spin state S_z=-5/2). This confirms that, as expected for a Mn spin dependent phenomena, reversing the polarization of detection from co-circular to cross-circular (Fig.9(c) and (d)) reverses the role played by the high and low energy lines of X_2-Mn: an identical strong increase of population is observed on S_z=+5/2 or S_z=-5/2 for a slightly detuned excitation on the corresponding X-Mn states.

These experimental results show that the resonant CW excitation decreases the population of the spin state which is resonantly excited as expected from previous resonant optical pumping experiments[28]. More surprisingly, a slight detuning of the resonant CW laser increases significantly the Mn spin population in the state which is optically addressed. We will see in the following that this *spin population trapping* is a specific signature of the coherent dynamics of the Mn spin coupled with its nuclear spin and the resonant laser field.

To model the influence of a resonant laser field on the spin dynamics of a Mn atom embedded in a QD, we start from the analysis of the spin structure of a Mn atom in a strained zinc-blend semiconductor matrix. The Hamiltonian of the coupled electronic and nuclear spins of a Mn atom is given by equation (1). Different S_z of the Mn are coupled by the non-diagonal terms of H_{Mn}. For instance, the hyperfine terms $\mathcal{A}$ couples two consecutive Mn spin states through an electron-nuclei flip-flop. We could then expect that a non-equilibrium population of the electronic spin prepared optically would be transferred to the nuclear spin. This would lead to an optical pumping of the nuclear spin of the Mn. However, in the presence of a large magnetic anisotropy, these electron-nuclei flip-flops are blocked.

An anisotropic strain distribution in the QD plane can also efficiently couple Mn spin states S_z separated by two units through the crystal field term $E(S_x^2 - S_y^2)$. As we will see, all these coupling terms affect the population redistribution on the six Mn spin states under resonant optical pumping.

The coupling with a resonant laser field can be used to tune the energy of one selected Mn spin state across the full fine structure of the Mn atom[41]. This allows in particular to restore the degeneracy of two consecutive Mn spins states giving an optical way to control the flip-flops of the electronic and nuclear spins. The energy tuning of the optically dressed states is then expected to influence the dynamics of the coupled electronic and nuclear spins. To estimate this effect, we calculated the coherent evolution of coupled electronic and nuclear spins optically coupled to an X-Mn state.

As illustrated in Fig. 10, we first consider that a single exciton state ($|J_z = -1\rangle$) is laser coupled to one state

of the Mn ($|S_z = +5/2, I_z\rangle$) with a Rabi energy $\hbar\Omega_R$. This approximation is justified in strongly confined QDs with a large X-Mn splitting resonantly excited by a narrow band laser and in the limit of small laser detuning. The exciton has a pure dephasing rate γ_d and the relaxation of the Mn spin in the ground state (empty QD) is described by a relaxation rate Γ_{Mn} coupling one by one the different electronic spin states S_z. The nuclear spin I_z is considered to be frozen in the timescale of all the spin preparation mechanism discussed here.

The X-Mn complex can relax its energy along a Mn spin conserving channel at rate Γ_r (optical recombination of X) or along channels including a relaxation of the Mn spin at rate $\Gamma_{relax} = 1/\tau_{relax}$: Γ_{relax} allows a transfer of population from the state $|J_z = -1, S_z = +5/2, I_z\rangle$ to any other spin state of the Mn S_z with I_z unchanged. This is a simplified effective way to describe the complex X-Mn spin dynamics at the origin of the optical pumping mechanism[40,47]. At magnetic fields lower than a few hundreds mT, we also consider that the Zeeman energy of the X-Mn can be neglected since it is much smaller than the X-Mn exchange interaction: we only take into account the effect of the magnetic field on the empty QD (Last term of Hamiltonian (1) for a Mn alone).

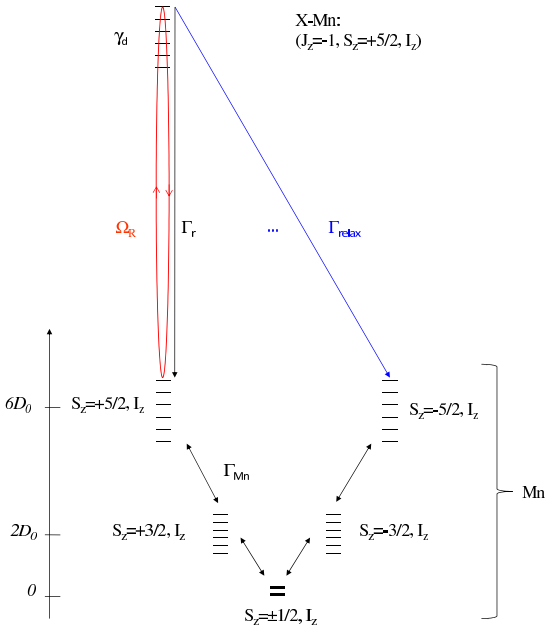

FIG. 10: Scheme of the energy levels and transitions rates involved in the resonant excitation model (see text). $\hbar\Omega_R$ is the energy coupling with the laser, $\gamma_d = 1/\tau_d$ is a pure dephasing rate of the exciton, $\Gamma_{Mn} = 1/\tau_{Mn}$ is the spin relaxation rate of the Mn, $\Gamma_r = 1/\tau_r$ is the optical recombination rate of the exciton. A relaxation rate of the exciton-Mn complex $\Gamma_{relax} = 1/\tau_{relax}$ is used for an effective description of the optical pumping effect.

Using the simplified level scheme presented in Fig.10, we can calculate the time evolution of the 42x42 density matrix ϱ describing the population and the coherence of the 36 states of the Mn alone (empty QD described by $\mathcal{H}_{Mn}$) and the 6 X-Mn states $|J_z = -1, S_z = +5/2, I_z\rangle$. The master equation which governs the evolution of ϱ can be written in a general form (Lindblad form) as:

$$\frac{\partial \varrho}{\partial t} = -i/\hbar[\mathcal{H}, \varrho] + L\varrho \qquad (2)$$

$\mathcal{H}$ is the Hamiltonian of the complete system (Mn and X-Mn) and $L\varrho$ describes the coupling or decay channels resulting from an interaction with the environment[48]. One can split $L\varrho$ in three parts:

1- The population transfer from level j to level i in an irreversible process associated with a coupling to a reservoir is described by $L_{inc,j\to i}\varrho$:

$$L_{inc,j\to i}\varrho = \frac{\Gamma_{j\to i}}{2}(2|i\rangle\langle j|\varrho|j\rangle\langle i| - \varrho|j\rangle\langle j| - |j\rangle\langle j|\varrho) \qquad (3)$$

where $\Gamma_{j\to i}$ is the incoherent relaxation rate from level j to level i. This operator describes the radiative decay of the exciton (irreversible coupling to the photon modes) or the relaxation of the Mn spin (irreversible coupling to the phonon modes). Such term could also be used to describe the optical generation of an exciton in the low excitation regime where the energy shift induced by the strong coupling with the laser field is neglected.

2- Pure dephasing, *i.e.*, phase relaxation not related to an exchange of energy with a reservoir, is also introduced for the exciton and described by $L_{deph,jj}\varrho$:

$$L_{deph,jj}\varrho = \frac{\gamma_{jj}}{2}(2|j\rangle\langle j|\varrho|j\rangle\langle j| - \varrho|j\rangle\langle j| - |j\rangle\langle j|\varrho) \qquad (4)$$

where γ_{jj} is a pure dephasing rate.

3- For a general description, valid from the low to the high optical excitation intensity regime, we consider that the laser field induces a coherent coupling between the ground and exciton states. The coherent coupling between two levels induced by the laser field leads to Rabi oscillations between the populations ϱ_{ii} and ϱ_{jj} and coherence of these levels $\varrho_{ij} = \varrho^*_{ji}$. In the Lindblad equation (2), this reversible coupling can be described by $L_{coh,i\leftrightarrow j}$:

$$L_{coh,i\leftrightarrow j}\varrho = i\frac{\Omega_{ij}}{2}(|j\rangle\langle i|\varrho + |i\rangle\langle j|\varrho - \varrho|j\rangle\langle i| - \varrho|i\rangle\langle j|) \qquad (5)$$

where $\hbar\Omega_{ij} = \mathcal{P}_{ij}\mathcal{E}$ is the Rabi energy splitting with $\mathcal{P}_{ij}$ the dipolar moment of the QD transition and $\mathcal{E}$ the amplitude of the electric field of the resonant CW laser. This term, which corresponds to the dipole-field coupling $-\overrightarrow{\mathcal{P}_{ij}}.\overrightarrow{\mathcal{E}} = -\hbar\Omega_{ij}(|j\rangle\langle i| + |i\rangle\langle j|)/2$, could also be included in the Hamiltonian evolution (first term of equation (2))[48,49].

The calculated evolution of the population of the different spin states of the Mn with the detuning of a circularly polarized laser around $|J_z = -1, S_z = +5/2, I_z\rangle$ is

presented in Fig. 11 for different Rabi energies. The detuning δ is defined as $\delta = \hbar\omega_0 - \hbar\omega_l$ with $\hbar\omega_0$ the energy of the optical excitonic transition and $\hbar\omega_l$ the energy of the CW laser[48]. The states $|S_z = +5/2, I_z\rangle$ of the Mn are coupled by the CW resonant laser to the X-Mn states $|J_z = -1, S_z = +5/2, I_z\rangle$ and we neglect the possible excitation of more than one exciton state by the resonant laser (i.e. the splitting between the X-Mn lines is larger than the Rabi energy or the detuning of the laser). At low Rabi energies and zero detuning, a strong decrease of the population of S_z=+5/2 and an increase of the population of the other spin states is observed: this corresponds to the expected optical pumping of the state S_z=+5/2. As the laser is slightly detuned on the high energy side of the transition, $\delta < 0$, a strong increase of the S_z=+5/2 population and simultaneous decrease of the S_z=±1/2 population is observed. This detuning dependence, that we call *spin population trapping*, is very similar to the experimental data.

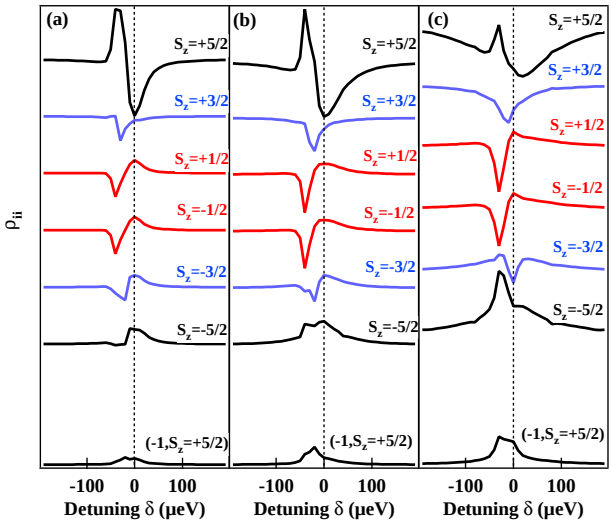

FIG. 11: Calculated population of the six electronic spin states of a Mn versus the detuning δ of the CW control laser around the X-Mn state $|J_z = -1, S_z = +5/2, I_z\rangle$ for different Rabi energies: (a) $\hbar\Omega_R = 12.5\mu eV$, (b) $\hbar\Omega_R = 25\mu eV$ and (c) $\hbar\Omega_R = 50\mu eV$. The relaxation times are $\tau_{Mn} = 250ns$, $\tau_r = 0.25ns$, $\tau_{relax} = 60ns$, $\tau_d = 100ps$ and the Mn fine structure parameters $\mathcal{D}_0 = 7\mu eV$ and $E = 0.35\mu eV$.

The calculation shows that the states S_z=+5/2 (excited by the CW resonant laser) and S_z=±1/2 are the most affected by the laser detuning (see for instance Fig. 11(b)). Let us give a qualitative description of the observed complex spin dynamics. As the CW laser is detuned on the high energy side of the transition, the optically dressed states associated with S_z=+5/2 can be pushed on resonance with S_z=±1/2. At resonance, mixed states of S_z=+1/2 and S_z=+5/2 are created through the anisotropic crystal field (E term of equation (1)). This coherent coupling produces an enhancement of the population transfer between S_z=+1/2 and the optically dressed states associated with S_z=+5/2.

The optical recombination of the optically dressed state, which is mainly an excitonic state, induces an irreversible transfer of population from S_z=+1/2 to S_z=+5/2. In addition, S_z=+1/2 and S_z=-1/2 are coherently coupled by the hyperfine interaction which, through electron-nuclei flip-flops, produces an oscillation of population between these two levels. This oscillation is interrupted by the irreversible transfer of S_z=+1/2 to the optically dressed states. Consequently, both the S_z=+1/2 and the S_z=-1/2 populations are transferred to S_z=+5/2. This mechanism can explain the strong increase of the S_z=+5/2 (or S_z=-5/2) population for a circularly polarized CW laser excitation slightly detuned around the high or the low energy line of X-Mn.

The spectral width of the pumping signal (i.e. decrease of population obtained on the resonance with the transition) increases with the Rabi energy. Consequently, the optical pumping significantly affects the population trapping mechanism and a more complex dynamics is expected at hight excitation intensity (calculation presented in Fig. 11(c) for $\hbar\Omega_R = 50\mu eV$, larger than the excitation intensity used in the experiments presented here). In this high excitation regime, the population of S_z=±1/2 is transferred to S_z=+5/2 by the population trapping mechanism and simultaneously, the optical pumping empties S_z=+5/2. This leads to a transfer from S_z=+5/2 and S_z=±1/2 to S_z=-3/2 and S_z=-5/2.

To summarize, the coupling with a resonant laser field strongly modifies the spin dynamics of a Mn atom inserted in a strained self-assembled QD. In addition to the standard optical pumping, the Mn spin can be trapped in the state which is optically excited. This mechanism of *spin population trapping* is controlled by the presence of a coherent coupling between the different Mn spin states S_z induced by an in-plane strain anisotropy. Such spin dynamics is not specific to a Mn atom and could be observed in other solid state and atomic spin systems provided that a coherent coupling between the spin sub-levels is present.

V. RESONANT OPTICAL PUMPING OF A MN SPIN IN A STRAIN FREE QUANTUM DOT

Studies of the spin dynamics of Mn atoms in self-assembled CdTe/ZnTe QDs show that the strain induced magnetic anisotropy, changing from dot to dot, blocks the electronic Mn spin along the QD growth direction[28,31,32]: the precession of the Mn spin in the hyperfine field of its nuclei or in a weak transverse magnetic field is quenched. As one aims at performing a fast optical coherent control of the spin of a magnetic atom, using for example the optical Stark effect[50,51] in a weak transverse magnetic field, the strain induced magnetic anisotropy of the Mn should be suppressed. Strain free Mn-doped QDs would also offer the possibility to externally tune the electron nuclei flip-flops with an applied magnetic field to prepare

the nuclear spin of the Mn atom.

To obtain strain free magnetic QDs, we developed thin unstrained CdTe/CdMgTe quantum wells (QWs) doped with a low density of Mn atoms and lattice matched on a CdTe substrate. In these structures, localization of the carriers in the QW plane is achieved thanks to thickness fluctuations of the QWs at the monolayer scale[27]. A low density of Mn atoms is introduced during the quantum well growth and interface fluctuation islands containing individual Mn spins are obtained and optically probed using micro-spectroscopy techniques[52].

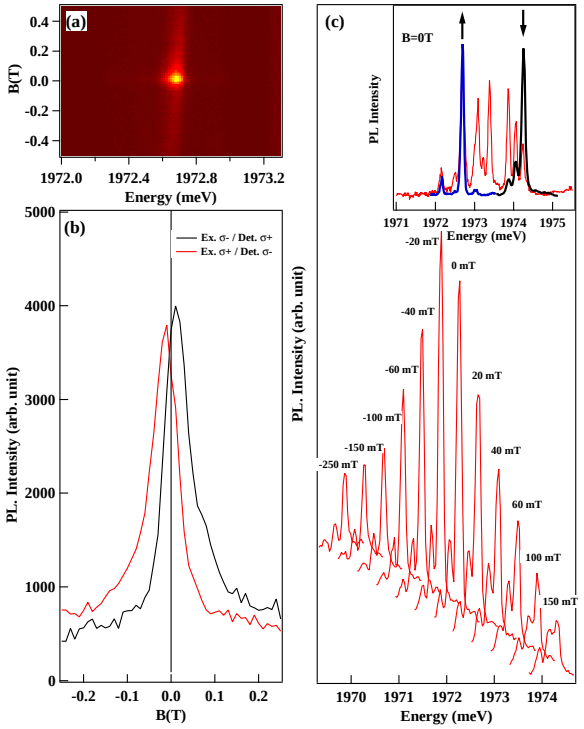

FIG. 12: Longitudinal magnetic field dependence of the intensity of the resonant PL in a strain-free Mn doped QD for crossed circular excitation and detection on the high and low energy lines respectively. (a) Intensity map of the magnetic field dependence of the resonant PL. (b) Magnetic field dependence of the resonant PL intensity for $\sigma-$ excitation / $\sigma+$ detection (black) and $\sigma+$ excitation / $\sigma-$ detection (red). (c) PLE detected on the low energy line for a $\sigma+$ excitation / $\sigma-$ detection and different longitudinal magnetic fields (the curves are horizontally and vertically shifted for clarity). The inset presents the non-resonant PL (red), the resonant PL for an excitation on the high energy line (blue) and the PLE detected on the low energy line (black) at B=0T. Arrows indicate the excitation/detection configuration for the resonant-PL experiments.

The weak value of the crystal field splitting of the Mn expected in these strain free QDs is revealed by the longitudinal magnetic field dependence of the resonant PL intensity. As presented in figure 12, for a cross circularly polarized excitation and detection on the high and low energy lines of X-Mn (i.e. excitation and detection of the same Mn spin state S_z=+5/2 or S_z=-5/2), a significant intensity of resonant PL is only observed for a longitudinal magnetic field lower than a few tens of mT. As a magnetic field is applied in the Faraday configuration, the resonant PL intensity abruptly decreases (Fig. 12(a)). A clear asymmetry is also observed in the magnetic field dependence of this resonant PL signal around zero Tesla. Under $\sigma-$ excitation on the high energy line and $\sigma+$ detection on the low energy line (*i.e.* excitation and detection of S_z=-5/2), the maximum of resonant PL intensity is slightly shifted towards positive magnetic fields and the decrease of the intensity is faster for negative magnetic fields (black curve in Fig. 12(b)). The situation is reversed for swapped excitation/detection circular polarizations (red curve in Fig. 12(b)).

This magnetic field dependence of the resonant PL intensity is a consequence of the fine and hyperfine structure of the Mn atom on its optical pumping. To model this behaviour we consider the dynamics of the coupled electronic and nuclear spins of the Mn in a possible residual crystal field. The fine and hyperfine Hamiltonian of the Mn is given by equation (1). Different S_z of the Mn are coupled by the non-diagonal terms of $\mathcal{H}_{Mn}$. The hyperfine terms $\mathcal{A}$ couples two consecutive Mn spin states through an electron-nuclei flip-flop. An anisotropy of the Mn site also couples Mn spin states S_z separated by two units through the crystal field term $E(S_x^2 - S_y^2)$. In the absence of magnetic anisotropy (weak value of D_0), all these coupling terms at zero magnetic field prevent the optical pumping of the electronic Mn spin.

The dynamics of the coupled electronic and nuclear spins of the Mn is controlled by the time evolution of $\mathcal{H}_{Mn}$ and the electronic Mn spin relaxation time τ_{Mn}. The nuclear spin relaxation is considered to be longer than the timescale of all the other spin relaxation mechanism discussed here. To describe the magnetic field dependence of the resonant PL, we extend the model presented in the previous section[44]. Under $\sigma-$ excitation on the high energy line, the exciton states $|X_z = -1, S_z = -5/2, I_z\rangle$ are laser coupled to the Mn states $|S_z = -5/2, I_z\rangle$. For a general description, valid from the low to the high optical excitation intensity regime, we consider that the resonant laser field induces a coherent coupling between the ground Mn spin state and the exciton state described by a Rabi energy $\hbar\Omega_R$. A pure dephasing time τ_d (*i.e.* not related to an exchange of energy with a reservoir) is introduced for the exciton state. The X-Mn complex can relax its energy along a Mn spin conserving channel with a characteristic time τ_r (optical recombination of X) or along channels including a relaxation of the Mn spin with a spin flip time τ_{relax}. The parameter τ_{relax} is a simplified effective way to describe the complex X-Mn spin dynamics at the origin of the optical pumping mechanism[40,47].

With this level scheme (Fig. 10), we can compute the steady state population of the resonantly excited exciton level $\rho_{|X_z=-1,S_z=-5/2\rangle}$[44]. This population is proportional to the intensity measured in the resonant PL

experiment. The evolution under longitudinal magnetic field of the calculated population of the exciton states $|X_z = -1, S_z = -5/2\rangle$ is presented in Fig. 13 for different values of the crystal field anisotropy D_0 and with E=$D_0/3$. We chose E=$D_0/3$ to obtain the maximum rhombic splitting and no preferential axial symmetry for the Mn environment[53]. The main feature of the magnetic field dependence of the resonant PL observed experimentally (*i.e.* the width, the asymmetry and shift of the maximum from B=0T) can be well reproduced with D_0 in the 1-2μeV range (Fig. 13(a)).

For a qualitative understanding of the behaviour of the resonant PL, we can look at the magnetic field dependence of the fine and hyperfine structure of the Mn atom (Fig. 13(c)). For a negative magnetic field, the state S_z=-5/2 is shifted away from the other Mn spin states: the precession of the Mn spin induced by the non-diagonal terms of $\mathcal{H}_{Mn}$ is blocked, the optical pumping is restored within a few mT and the resonant PL signal decreases abruptly. For a positive magnetic field of a few mT, the state S_z=-5/2 is pushed to lower energy across the other Mn spin states. All the non-diagonal terms of $\mathcal{H}_{Mn}$ (a, $\mathcal{A}$ and E terms) mix the different S_z and prevent the optical pumping of the electronic spin of the Mn. To restore the optical pumping, a larger positive magnetic field is needed. This explains that for a resonant excitation on S_z=-5/2, the drop of the resonant PL intensity is slower for positive magnetic fields. The magnetic field dependence is reversed for an optical excitation of S_z=+5/2 (*i.e.* opposite circular polarization for the excitation). For large positive or negative magnetic fields, the Zeeman splitting of the Mn (controlled by g_{Mn}=2) dominates all the crystal field terms and the hyperfine coupling. The Mn spin is quantized along the direction of the applied magnetic field, the optical pumping efficiency increases and the resonant PL vanishes.

Mn atoms are introduced in a thin CdTe layer that is coherently grown on a CdTe substrate. The first expectation would be that D_0=0 and that the dynamics of the Mn spin would be controlled by its intrinsic fine and hyperfine structure (a and $\mathcal{A}$ terms). However, as shown in Fig. 13(b), all the non-diagonal terms of $\mathcal{H}_{Mn}$ contribute to the amplitude of the resonant PL signal. A residual crystal field in the μeV range has to be introduced in the model to explain the asymmetry observed in the experimental resonant PL data. For an axial crystal field (*i.e.* E=0), the calculated magnetic field dependence of the resonant PL is narrower than in the experiment (Fig. 13(b)). This suggests that the remaining small crystal field felt by the Mn atom in our structure has no axial symmetry but arises from a more disordered environment. This crystal field could arise from an alloy composition fluctuation around the Mn atom. One should keep in mind that the Mn atoms are located in a CdTe layer that is only 4 monolayers thick and surrounded by $Cd_{0.7}Mg_{0.3}Te$ barriers. A Mn atom interacting with a confined exciton is always close to the barrier and the substitution of some Cd atoms by Mg atoms in the vicinity of the Mn reduces the symmetry of the local electric field and can induce weak crystal field terms D_0 and E[54,55]. While further investigations would be needed to fully understand this point, we observe that D_0 is positive as one could expect from the lattice parameter difference between MgTe and CdTe: MgTe has a smaller lattice parameter than CdTe, so the presence of a Mg atom in the vicinity of the Mn induces a local

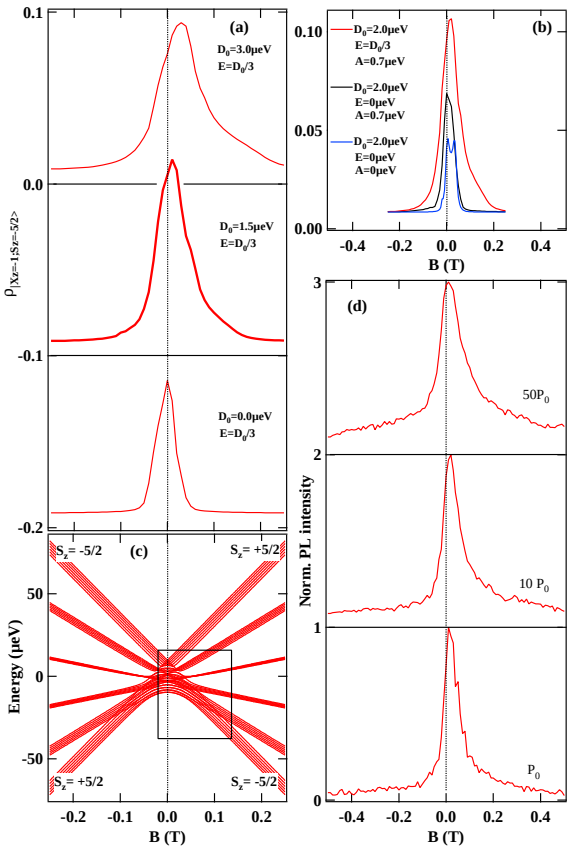

FIG. 13: (a) Modelling of the longitudinal magnetic field dependence of the population of the exciton state $|X_z = -1, S_z = -5/2\rangle$ under resonant excitation for different values of the crystal field terms D_0 and E=$D_0/3$ (the curves are vertically shifted for clarity). The population of this level is proportional to the resonant PL signal. The parameters used in the calculation (see text for details) are $\hbar\Omega_R = 15\mu eV$, $\tau_{Mn} = 100ns$, $\tau_r = 0.3ns$, $\tau_{relax} = 50ns$, $\tau_d = 100ps$, $A = 0.7\mu eV$, $a = 0.32\mu eV$ and $g_{Mn} = 2$. (b) Calculated population of the exciton state $|X_z = -1, S_z = -5/2\rangle$ for D_0=2μeV and E=$D_0/3$ (red), E=0 (black), E=0 and $A = 0$ (blue). (c) Calculated fine and hyperfine structure of a Mn spin with $A = 0.7\mu eV$, $a = 0.32\mu eV$, $g_{Mn} = 2$, D_0=1.5μeV and E=$D_0/3$. The black rectangle highlights the magnetic field range where the state S_z=-5/2 significantly interacts with the other Mn spin states. (d) Experimental magnetic field dependence of the resonant PL signal for different excitation intensities and $\sigma-$ excitation / $\sigma+$ detection on the high and low energy lines respectively. The curves are normalized and vertically shifted for clarity.

reduction of the lattice parameter and then a positive crystal field term[36].

As presented in Fig. 13(d), the magnetic field dependence of the resonant PL is observed in a broad range of excitation intensities. However, the width of the resonant PL peak and the residual background of resonant PL increase with the increase of the excitation intensity. This reflects a reduction of the optical pumping efficiency at high excitation power. This reduction at high excitation power is likely due to a perturbation of the Mn spin by the additional non-resonant injection of free carriers that destroys the Mn spin memory[23].

To summarize, in these strain free structures, an isolated Mn atom experiences a residual weak crystal field splitting likely due to local alloy fluctuations. This contrasts with self-assembled QDs where the Mn spin is split by a large magnetic anisotropy induced by the biaxial strains in the QD plane. Consequently, in self-assembled QDs, an efficient optical pumping of the Mn spin is observed at zero magnetic field whereas a weak magnetic field in the Faraday geometry has to be applied on strain-free QDs to restore a Mn spin memory. Despite this residual crystal field, strain free magnetic QDs is a promising system to probe the coherent dynamics of the coupled electronic and nuclear spins of a Mn atom in zero or weak magnetic field.

VI. CONCLUSION

It has been demonstrated during the last years that the atomic-like optical properties of semiconductor QDs could be efficiently used to control the spin state of individual magnetic atoms. We have shown here that a Mn atom incorporated in a neutral II-VI semiconductor self-assembled QD presents a magnetic anisotropy of a few tens of μeV resulting from a strained induced modification of the local crystal field. This magnetic anisotropy is responsible for the Mn spin memory of a few μs observed at zero magnetic field. The fine structure splitting of the Mn spin can be modified optically and the coupling with a resonant laser field strongly modifies the spin dynamics of the Mn atom. The magnetic anisotropy of the Mn decreases significantly in strain-free QDs. Strain free Mn-doped QDs could be included in photonic structures such as optical planar micro-cavities to increase the number of collected photons and increase the interaction of the QDs with light. This would open the possibility to realize in the near future an optical coherent control of an individual Mn spin in a weak transverse field using the optical Stark effect or to probe and control the dynamics of the nuclear spin of the Mn atom.

The use of semiconductor hetero-structures doped with magnetic impurities offers a large flexibility for the realization of single spin devices. The intrinsic properties of the semiconductors permit either an optical or an electrical access to individual spins. Band gap and strain engineering as well as a control of the QD charge permit to tune the magnetic atom environment. For instance, it is expected that a Mn atom could develop a large anisotropy energy in the meV range when it is exchange coupled with a single confined heavy-hole spin. This electrical control of the magnetic anisotropy makes these nanosized systems attractive for basic investigations as well as for miniaturized data storage applications. The large sensitivity of a magnetic atom spin to its local strain environment is also very promising for the realization of hybrid spin-nanomechanical systems. Among nanomechanical systems, hybrid systems are a specific class for which a nanomechanical oscillator is coupled to an individual quantum system, such as a solid state spin qubit[56]. Such systems could provide a way to prepare and detect non-classical states of mechanical motion offering various applications in the context of quantum information such as the storage of a qubit in the mechanical state of an oscillator. Finally, let's note that many others magnetic elements could be included in II-VI magnetic QDs: For instance, Cr with 90 % of isotopes without nuclear spin could be an interesting candidate to obtain long spin coherence time.

Acknowledgments

The work presented here was realized in the framework of the CEA (INAC) / CNRS (Institut Néel) joint research team "NanoPhysique et SemiConducteurs".

* Electronic address: lucien.besombes@grenoble.cnrs.fr

[1] P. M. Koenraad and M. E. Flatte, Nature Materials **10**, 91 (2011).
[2] J. Seufert, G. Bacher, M. Scheibner, A. Forchel, S. Lee, M. Dobrowolska, and J. K. Furdyna, Phys. Rev. Lett. **88**, 027402 (2001).
[3] J.K. Furdyna, J. Appl. Phys. **64** R29 (1988).
[4] J. Brossel and F. Bitter, Phys. Rev. **86**, 17308 (1952).
[5] M. Atatüre, J. Dreiser, A. Badolato, A. Högele, K. Karrai and A. Imamoglu, Science **312**, 551 (2006).
[6] B. D. Gerardot, D. Brunner, P. A. Dalgarno, P. Ohberg, S. Seidl, M. Kroner, K. Karrai, N. G. Stoltz, P. M. Petroff and R. Warburton, Nature **451**, 441 (2008).
[7] B. R. Mollow, Phys. Rev. A 5, 2217 (1972).
[8] G. Jundt, L. Robledo, A. Högele, S. Falt and A. Imamoglu, Phys. Rev. Lett. **100**, 177401 (2008).
[9] X. Xu, B. Sun, P.R. Berman, D.G. Steel, A.S. Bracker, D. Gammon and L.J. Sham, Science **317**, 929 (2007).
[10] X. Xu, B. Sun, E. D. Kim, K. Smirl, P.R. Berman, D.G. Steel, A.S. Bracker, D. Gammon and L.J. Sham, Phys. Rev. Lett. **101**, 227401 (2008).
[11] M. Kroner, C. Lux, S. Seidl, A. W. Holleitner, K. Kar-

rai, A. Badolato, P. M. Petroff and R.J. Warburton, Appl. Phys. Lett. **92**, 031108 (2008).
[12] A. Muller, W. Fang, J. Lawall and G.S. Solomon, Phys. Rev. Lett. **101**, 027401 (2008).
[13] L. Besombes, Y. Leger, L. Maingault, D. Ferrand, H. Mariette and J. Cibert, Phys. Rev. Lett. **93**, 207403 (2004).
[14] L. Besombes, C.L. Cao, S. Jamet, H. Boukari and J. Fernandez-Rossier, Phys. Rev. B **86**, 165306 (2012).
[15] A. Kudelski, A. Lemaitre, A. Miard, P. Voisin, T.C.M. Graham, R.J. Warburton and O. Krebs, Phys. Rev. Lett. **99**, 247209 (2007).
[16] Olivier Krebs, Emile Benjamin, and Aristide Lematre, Phys. Rev. B **80**, 165315 (2009)
[17] O. Krebs and A. Lemaitre, Phys. Rev. Lett. **111**, 187401 (2013).
[18] J. Kobak, T. Smolenski, M. Goryca, M. Papaj, K. Gietka, A. Bogucki, M. Koperski, J.-G. Rousset, J. Suffczynski, E. Janik, M. Nawrocki, A. Golnik, P. Kossacki, W.Pacuski, Nature Com. **5**, 3191 (2014).
[19] J. Fernandez-Rossier, Phys. Rev. B **73**, 045301 (2006).
[20] A. H. Trojnar, M. Korkusiski, E. S. Kadantsev, P. Hawrylak, M. Goryca, T. Kazimierczuk, P. Kossacki, P. Wojnar, and M. Potemski, Phys. Rev. Lett. **107**, 207403 (2011).
[21] A. H. Trojnar, M. Korkusinski, M. Potemski and P. Hawrylak, Phys. Rev. B **85**, 165415 (2012).
[22] A. H. Trojnar, M. Korkusinski, U. C. Mendes, M. Goryca, M. Koperski, T. Smolenski, P. Kossacki, P. Wojnar, P. Hawrylak, Phys. Rev. B **87**, 205311 (2013).
[23] L. Besombes, Y. Leger, J. Bernos, H. Boukari, H. Mariette, J.P. Poizat, T. Clement, J. Fernandez-Rossier and R. Aguado, Phys. Rev. B **78** 125324 (2008).
[24] M. Koperski, M. Goryca, T. Kazimierczuk, T. Smoleski, A. Golnik, P. Wojnar, and P. Kossacki, Phys. Rev. B **89**, 075311 (2014).
[25] Bacher G., Maksimov A. A., Schömig H., Kulakovskii V. D., Welsch M. K., Forchel A., Dorozhkin P. S., Chernenko A. V., Lee S., Dobrowolska M., Furdyna J. K., Phys. Rev. Lett. **89**, 127201 (2002).
[26] P. Wojnar, C. Bougerol, E. Bellet-Amalric, L. Besombes, H. Mariette and H. Boukari, J. Crystal Growth **335**, 28 (2011).
[27] L. Besombes, K. Kheng and D. Martrou, Phys. Rev. Lett. **85**, 425 (2000).
[28] C. Le Gall, R. S. Kolodka, C. L. Cao, H. Boukari, H. Mariette, J. Fernandez-Rossier and L. Besombes, Phys. Rev. B **81**, 245315 (2010).
[29] M.M. Glazov, E.L. Ivchenko, L. Besombes, Y. Leger, L. Maingault, H. Mariette, Phys. Rev. B **75**, 205313 (2007).
[30] A. O. Govorov, A. V. Kalameitsev, Phys. Rev. B **71**, 035338 (2005).
[31] C. Le Gall, L. Besombes, H. Boukari, R. Kolodka, J. Cibert and H. Mariette, Phys. Rev. Lett. **102**, 127402 (2009).
[32] M. Goryca, T. Kazimierczuk, M. Nawrocki, A. Golnik, J. A. Gaj, P. Kossacki, P. Wojnar and G. Karczewski, Phys. Rev. Lett. **103**, 087401 (2009).
[33] E. Baudin, E. Benjamin, A. Lemaitre, O. Krebs, Phys. Rev. Lett. **107**, 197402 (2011).
[34] I. A. Akimov, R. I. Dzhioev, V. L. Korenev, Yu. G. Kusrayev, V. F. Sapega, D. R. Yakovlev, and M. Bayer, J. Appl. Phys. **113** 136501 (2013).
[35] M. Qazzaz, G. Yang, S.H. Xin, L. Montes, H. Luo and J.K. Furdyna, Solid State Communications **96**, 405 (1995).
[36] M.T. Causa, M. Tovar, S.B. Oseroff, R. Calvo and W. Giriat, Phys. Lett. **A77**, 473 (1980).
[37] S. Cronenberger, M. Vladimirova, S. V. Andreev, M. B. Lifshits and D. Scalbert, Phys. Rev. Lett. **110**, 077403 (2013).
[38] T. Strutz, A. M. Witowski, and P. Wyder, Phys. Rev. Lett. 68, 3912 (1992).
[39] T. Dietl, P. Peyla, W. Grieshaber and Y. Merle d'Aubigne, Phys. Rev. Lett., **74**, 474 (1995).
[40] C. L. Cao, L. Besombes and J. Fernandez-Rossier, Phys. Rev. B **84**, 205305 (2011).
[41] C. Le Gall, A. Brunetti, H. Boukari and L. Besombes, Phys. Rev. Lett. **107**, 057401 (2011).
[42] S.H. Autler and C. H. Townes, Phys. Rev. **100**, 703 (1955).
[43] S.J. Boyle, A.J. Ramsay, A.M. Fox, M.S. Skolnick, A.P. Heberle and M. Hopkinson, Phys. Rev. Lett. **102**, 207401 (2009).
[44] S. Jamet, H. Boukari and L. Besombes, Phys. Rev. B **87**, 245306 (2013).
[45] T. Flissikowski, A. Betke, I.A. Akimov and F. Henneberger, Phys. Rev. Lett. **92**, 227401 (2004).
[46] L. Besombes, Y. Leger, L. Maingault, D. Ferrand, H. Mariette and J. Cibert, Phys. Rev. B **71**, 161307 (2005).
[47] L. Cywinski, Phys. Rev. B **82**, 075321 (2010).
[48] M.P. van Exter, J. Gudat, G. Nienhuis and D. Bouwmeester, Phys. Rev. A **80**, 023812 (2009).
[49] C. Roy and S. Hughes, Phys. Rev. X **1**, 021009 (2011).
[50] D.E. Reiter, T. Kuhn and V.M. Axt, Phys. Rev. B **85**, 045308 (2012).
[51] D.E. Reiter, V.M. Axt, T. Kuhn, Phys. Rev. B **87**, 115430 (2013).
[52] L. Besombes and H. Boukari, Phys. Rev. B **89**, 085315 (2014).
[53] D. Gatteschi, R. Sessoli, J. Villain, Molecular nanomagnets, Oxford University Press (2006).
[54] D.L. Griscom and R.E. Griscom, The Journal of Chemical Physics **47**, 2711 (1967).
[55] Z. Wang, W. Zheng, J. van Tol, N. S. Dalal, G. F. Strouse, Chemical Physics Letters **524**, 73 (2012).
[56] O. Arcizet, V. Jacques, A. Siria, P. Poncharal, P. Vincent, S. Seidelin, Nature Physics **7**, 879 (2011).